Research Square

Preprints are preliminary reports that have not undergone peer review.
They should not be considered conclusive, used to inform clinical practice,
or referenced by the media as validated information.

Receptor allocation, not receptor abundance: sensory-neuron CALCRL transcripts are partnered by different RAMPs in human, macaque and mouse

Tianjiao Li
Beijing Chao-Yang Hospital, Capital Medical University
Yuhan Liu
Hebei Medical University
Lingxuan Li
Beijing Forestry University
Chenwei Li
The 989th Hospital of the Joint Logistic Support Force of PLA
Ye Li
Chinese PLA General Hospital
Chaodong Wang
Beijing Chao-Yang Hospital, Capital Medical University
Yun Wang
Beijing Chao-Yang Hospital, Capital Medical University
Yonghong Liu
Xijing Hospital, Air Force Medical University
Bo Sun
sunnyboo_traci@163.com

Beijing Chao-Yang Hospital, Capital Medical University

Research Article

Keywords: CALCRL, RAMP, CGRP receptor, adrenomedullin receptor, sensory ganglia, single-cell RNA sequencing, cross-species difference

Posted Date: November 12th, 2026

DOI: https://doi.org/10.21203/rs.3.rs-11508950/v1

License: This work is licensed under a Creative Commons Attribution 4.0 International License.
Read Full License

Additional Declarations: No competing interests reported.

Receptor allocation, not receptor abundance: sensory-neuron CALCRL transcripts are partnered by different RAMPs in human, macaque and mouse

Tianjiao Li[1,2], Yuhan Liu[3], Lingxuan Li[4], Chenwei Li[5], Ye Li[6], Chaodong Wang[1], Yun Wang[1,‡], Yonghong Liu[7,‡], Bo Sun[1,‡]

‡ Corresponding authors.

[1] Department of Neurology, Beijing Chao-Yang Hospital, Capital Medical University, Beijing, China

[2] Haidian No. 58 Cadre Sanatorium, Retired Cadres Service Administration Bureau of the Chinese People's Liberation Army in Beijing, Beijing, China

[3] School of Stomatology, Hebei Medical University, Shijiazhuang, China

[4] Department of Psychology, College of Humanities and Social Sciences, Beijing Forestry University, Beijing, China

[5] Department of Neurology, The 989th Hospital of the Joint Logistic Support Force of PLA, Pingdingshan, China

[6] Department of Pain Medicine, The First Medical Center of Chinese PLA General Hospital, Beijing, China

[7] Department of Neurology, Xijing Hospital, Air Force Medical University, Xi'an, China

Corresponding author: Bo Sun, Department of Neurology, Beijing Chao-Yang Hospital, Capital Medical University, 8 Gongti Nanlu, Chaoyang District, Beijing, China. Email: sunnyboo_traci@163.com.

Co-corresponding authors: Yonghong Liu, Department of Neurology, Xijing Hospital, Air Force Medical University, Xi'an, China. Email: liuyhong@fmmu.edu.cn. Yun Wang, Department of Neurology, Beijing Chao-Yang Hospital, Capital Medical University, Beijing, China. Email: drdrwy@163.com.

Abstract

Background. Calcitonin receptor-like receptor (CALCRL) binds no ligand on its own: it must be partnered by a receptor activity-modifying protein (RAMP), and RAMP1, RAMP2 or RAMP3 turns it into the CGRP, AM1 or AM2 receptor. Receptor identity is therefore set not by how much CALCRL a neuron has but by how it divides that pool. Every approved CGRP-pathway drug targets this receptor or its ligand. Whether sensory neurons divide the pool the same way in humans and mice has not been measured.

Methods. We re-analysed public single-cell and single-nucleus RNA sequencing of human, macaque, mouse and rat trigeminal and dorsal root ganglia, anchored by a three-species series from one laboratory and one pipeline. The primary statistic compares two RAMPs within the same cell (paired exact McNemar), which cancels sequencing depth, capture efficiency and ambient RNA by construction. Detection floors, depth bins, preparation strata and an annotation-space audit were fixed before the data were read.

Results. In a depth-matched gate, mouse neurons allocate the pool to RAMP2 (within-cell odds ratio 25.15 for RAMP2 over RAMP3) and macaque neurons give it to RAMP3 (0.105), a 239-fold species × RAMP interaction ($z = -67.3$) that survives every preparation stratum and recurs in three further macaque datasets from one study. Human neurons follow RAMP3 in every dataset available, including all nine of a 53,596-neuron reference atlas, where the paired odds ratio falls below parity everywhere and pools to 0.114 (95% CI 0.059–0.220, $I^2 = 98.8\%$); the direction is unambiguous but the magnitude is not, so we report a pooled interval rather than a single number.

The difference is a family-internal crossover, holds across cell types, and extends to satellite glia, where mouse allocates to RAMP2 (odds ratio 0.0019) while RAMP2 never exceeds 3.84% detection in any human glial gate.

Conclusions. The RAMP that partners CALCRL in sensory neurons is a species variable, graded across species with one qualitative step. Rodent pharmacology of "the sensory-neuron CGRP receptor" therefore reads it against a differently composed pool: AM1-dominated in mouse, AM2-dominated in primate neurons.

Keywords: CALCRL; RAMP; CGRP receptor; adrenomedullin receptor; sensory ganglia; single-cell RNA sequencing; cross-species difference

Background

Migraine is a disorder of sensory processing, and the trigeminal innervation of the cranial meninges is both where it starts and what treatment targets [1]. Those afferents release calcitonin gene-related peptide (CGRP) from their endings, and CGRP on its own provokes a migraine-like headache in susceptible people. Four decades of work on that loop produced the trigeminovascular framework most current therapy is designed around [2, 3].

The framework now has pharmacological support. Antibodies against the CGRP ligand reduce monthly migraine days in episodic and chronic migraine [4–6], as does an antibody against the receptor itself [7, 8], and small-molecule antagonists work acutely and, more recently, preventively [9–11]. American Headache Society guidance puts CGRP-targeted therapy among first-line preventive options [12]. The drugs work, and they work on a defined molecular entity.

They do not work on the entity the textbooks name. CGRP and its relatives activate no dedicated receptor protein. They activate calcitonin receptor-like receptor (CALCRL), which binds no ligand and does not reach the surface unless a receptor activity-modifying protein (RAMP) partners it. The partner sets the pharmacology: CALCRL with RAMP1 is the CGRP receptor, with RAMP2 the adrenomedullin AM1 receptor, with RAMP3 AM2 [13, 14], and the RAMP extracellular domain reshapes the CALCRL ligand pocket to make the switch [15]. One CALCRL gene therefore serves three receptors, and what decides which one a cell presents is how it splits that pool among the three RAMPs, not how much CALCRL it has.

Allocation is also the variable the system itself regulates. In the trigeminal ganglion the three RAMPs move as one coupled pool: across the mouse oestrous cycle Ramp1, Ramp2 and Ramp3 all vary while Calcrl does not, and in Ramp1-knockout mice the cyclical variation of Ramp2 and Ramp3 disappears [16]. A change in one RAMP therefore reports redistribution rather than a change in supply. Co-expressed RAMP3 suppresses a RAMP1-dependent CGRP response by 47% [17]. The corollary matters for how mouse models are built: substituting human RAMP1 leaves the rest of the pool free to reallocate, so a humanised-RAMP1 animal tests something narrower than it is usually taken to test [18].

The two non-canonical assemblies are not decorative. Adrenomedullin and adrenomedullin 2 belong to the same peptide family as CGRP, are expressed at sites that matter for migraine, and carry pro- and anti-nociceptive actions of their own, including direct effects on dorsal root ganglion neurons [19]; both are among the most frequently proposed non-CGRP targets for headache [20, 21]. RAMP variation is also visible in patients: a RAMP1 polymorphism has been associated with the transformation of episodic migraine into medication-overuse headache [22]. Yet which RAMP dominates a human sensory neuron has never been measured.

A PubMed search for RAMP2 or RAMP3 with trigeminal or dorsal root ganglion returns nine papers in total (October 2026). None of them, to our knowledge, reports the allocation of the CALCRL pool at single-cell resolution in human tissue. The mouse and rat literature is a handful of tissue-level studies averaging across neuronal, glial and vascular compartments [23–26]; the primate tissue work is limited in the same way [27]; and where species have been compared directly, the comparison was made on RAMP1 or on the calcitonin receptor

rather than on all three RAMPs [28]. A recent rat study adds sex as a further source of variation in the same four genes [29].

So whether human and mouse sensory neurons build the same receptor is an open question, and the drugs in clinical use make it urgent. Whole-ganglion methods could not have answered it even had the difference been there, because the glial and vascular compartments that carry much of the RAMP2 and RAMP3 signal dominate the average. The same limitation applies at the protein level: RAMP2 and RAMP3 have lacked antibodies validated for the purpose, which is one reason the question stayed open [30].

Methods

Datasets and data sources

Records came from a title-field search of GEO DataSets on 18 October 2026 (ganglion name plus single-cell or single-nucleus terms), returning 7 trigeminal and 14 dorsal root ganglion records, plus the accessions of the cross-species atlases we analysed, since a title query misses records deposited without those words. Inclusion required a deposited per-cell count matrix, a matched chromosome-level annotation and a preparation resolving neurons or glia individually; excluded were bulk or spatial data, integrated downsampled objects and scaffold-level gene models. Table S0 lists every record with its reason for exclusion.

We analysed public data only; accessions, platforms, sample counts and per-sample annotations are in Table S1 and under Availability of data and materials. Four datasets carry the main analysis: human trigeminal ganglion single-nucleus RNA sequencing (GSE197289, 3,873 neurons) [31], human dorsal root ganglion single-nucleus RNA sequencing (GSE168243, 1,770 neurons) [32], and the iPain mouse atlases (23,894 trigeminal and 117,284 dorsal root ganglion neurons) [33], whose source composition, accessions and suspension types are in Table S12.

These are anchored by GSE201654, in which macaque, human and mouse dorsal root ganglia were prepared, sequenced and quantified in one laboratory under one pipeline [34]. We used all 44 usable per-sample CellRanger matrices (macaque 16, human 18, mouse 10) rather than the deposited merged object, which is integrated and downsampled. A guinea-pig arm was retrieved and excluded before analysis because of a scaffold-level gene-model artefact inflating all four CALCRL-pathway genes (Table S26).

Four further groups address specific objections: three rhesus macaque resources from one laboratory, adding a second macaque species, a second laboratory and two chemistries [35]; a deeper human dorsal root ganglion dataset at single-soma resolution [36]; two human dorsal root ganglion resources with a glial compartment [37, 38]; and GSE169301, rat dorsal root ganglion on a whole-cell platform with six human single-nucleus libraries from the same study [39]. Its two arms are analysed separately, never against each other.

A fifth resource is the human dorsal root ganglion reference atlas released as a preprint by the PRECISION Human Pain Network. It is not deposited in GEO; we used the authors' public preprint release unmodified (61,817 features by 53,596 neurons, raw integer counts). Four of its nine contributing datasets, 43,020 neurons, do not overlap anything analysed above; the other five are re-used and never counted as independent replication. The release carries no donor field: `orig.ident` has 42 values but one placeholder accounts for 44,363 of the 53,596 neurons, leaving 30 samples with usable identities. Estimates from it are therefore made at dataset level, with the 30 identified samples as a secondary check, and no donor-level claim is made from it.

Definition of receptor assembly

Throughout, a receptor assembly means the CALCRL–RAMP heterodimer, and RAMP allocation means the relative frequency with which CALCRL is partnered by each RAMP in a defined cell population. Measurements

are transcript-level throughout. We did not measure protein, membrane localisation or signalling, and no statement below should be read as a claim about any of the three.

Allocation here is a population frequency, and the paralogues are sparse within a cell. In the mouse atlas 99.9% of trigeminal and 99.6% of dorsal root ganglion neurons score positive for none of the three RAMPs or for exactly one, and all three are co-detected in 29 of 117,284 dorsal root ganglion neurons (0.02%; Table S28); single-gene detection in the human arm of GSE201654 is likewise in the single digits (Table 1). The paired contrast therefore does not measure three proteins competing for one pool inside a cell. It treats cells in which two paralogues are scored at all as a matched design, so depth, capture efficiency and ambient RNA cancel, and counts those positive for one and not the other. Every quantity below is a count of cells.

Gating and cell-type definition

Gates were defined identically across species from markers rather than deposited labels, which can reflect doublets and do not compare between studies. Neurons were SNAP25+ and PRPH+; in the three-species series we also report an all-called-cells gate and a CALCA+ gate, the latter being the only gate in which all 18 human samples contribute with the three arms depth-matched to within 7% (Table S14). Glial gates were PLP1+, S100B+, SOX10+ and their unions and intersections, with the neuronal markers used to quantify doublet burden (Table S7). Vascular smooth muscle was Myh11+ and Cnn1+ with Calca, Tubb3 and Snap25 absent; endothelium was PECAM1+. The mouse ganglia differ in the size of these populations, so each compartment carries its own n. Subtypes were matched one-to-one between the iPain and GSE197289 taxonomies (NF1/2/3 to NF, PEP1/2 to PEP, cLTMR1/p_cLTMR2 to cLTMR) to hold composition constant (Table S5). Figure S8 draws the retained populations on the deposited atlas embedding for documentation only; no quantity here is measured from it.

Primary statistic: paired within-cell discordance

For each population we cross-tabulate, within the same cell, whether each of a pair of RAMPs was detected: b counts cells positive for the first RAMP only, c cells positive for the second only (Tables S2 and S2b). The odds ratio is c/b; the test is an exact binomial of min(b, c) against 0.5 among the b + c discordant cells, with intervals on the log odds ratio. Both genes being scored in the same cell, library size and per-cell capture cancel at the level of the individual cell, so no depth model, reference gene or spike-in is needed. Ambient contamination cancels only to the extent that the two paralogues carry the same ambient fraction, which is not testable here; a gene-specific soup contribution enters as bias rather than noise. The statistic is deliberately not a ratio of detection rates, which is depth-sensitive, and every row prints both discordant counts so direction never depends on remembering which RAMP is the numerator. Cells are nonetheless nested within samples and donors, so a cell-level p value describes consistency rather than strength of evidence; every estimate that carries weight is also reported at sample level, as per-sample discordant counts, a leave-one-out series and a bootstrap with the sample as resampling unit (Tables S16 and S24).

Controls fixed before analysis

Six controls were fixed before the data were read, and none was added after a result was seen. Detection floor: for single-soma and full-length chemistries a pair is reported only if both genes are detected in at least 5% of gated cells, which removes the RAMP1 and RAMP3 contrasts from two of the macaque resources (Table S19). It is not applied to 10x libraries, where low detection of the minor paralogue costs precision but not validity; the smallest 10x contrast this paper rests on carries 37 discordant cells, it is the human arm of the rat series, it is quoted with both counts and it is not pooled, and the two below 5%, RAMP2 at 0.51% in human dorsal root ganglion and 2.48% in human trigeminal ganglion, are likewise printed with both counts. Depth bins: cells are stratified by total UMI and each contrast recomputed within stratum, inside one chemistry (Table S3). Preparation strata: archival and nuclei-isolation methods vary within the series and are partly collinear with species, so every cross-species contrast is recomputed within each mixed stratum and inside an overlapping neuronal-purity window (Table S17).

Annotation space: each non-human matrix was checked against the genome its features are annotated to, since annotating a non-human library against the human transcriptome depresses RAMP2 relative to RAMP3 and can invert a within-cell contrast (Table S26). Counts came from raw, un-normalised matrices, and the two iPain objects were audited gene by gene on a 25-gene panel to confirm that log-normalised and raw matrices give the same detection counts (Table S9). Cell-type concordance: for each cell type in both species f = (RAMP1/RAMP2)human ÷ (RAMP1/RAMP2)mouse, which a constant platform bias would hold fixed. Study-level replication: every mouse analysis was repeated inside each contributing study, stratified by suspension type, with strata under 100 neurons reported separately rather than dropped (Table S4).

Pooling, heterogeneity and interaction tests

Because counting studies in the same direction quantifies direction but not magnitude, discordant counts were also pooled; per-source estimates are in Table S10 and the pooled models in Tables S13 and S15. Within a stratum the effect size is the within-cell log odds ratio $y = \ln(c/b)$ with variance $1/b + 1/c$, and no depth correction enters, for the same reason none enters the McNemar test; a stratum containing a zero gets a 0.5 continuity correction inside that stratum only and is flagged. Strata are combined by DerSimonian–Laird random effects with the fixed-effect estimate, Cochran's Q and I^2 beside it, and strata under 100 cells are excluded with the number stated. Species are compared as the difference of log odds ratios over the square root of the summed variances, which tests the species × RAMP interaction rather than comparing two significance tests. Two derived quantities are deliberately not reported: a ratio of two distances where one is indistinguishable from zero, whose interval crosses zero, the bound being reported instead; and a three-gene rank ordering, which can be carried by whichever two genes differ least. DerSimonian–Laird under-estimates between-stratum variance when k is small, as here (k = 2 to 7), so Q and I^2 accompany every pooled estimate and no pooled p value is offered as primary evidence.

Preparations and platforms

Most of the data are single-nucleus. Nuclear and whole-cell preparations differ systematically in which transcripts they recover [40], so every conclusion that depends on preparation names it, and the rat arm exists to test whether the rodent result survives whole-cell capture. On the human side the reference atlas [41] contributes one whole-cell SMART-seq2 library (1,598 somata, median 145,856 UMI) against roughly 52,000 nuclei, so the human preparation contrast is internal and small rather than absent.

The two pseudobulk CPM sets compared across species are not the same kind of average, and both are deposited. The human value is the pooled counts of all six GSE168243 neuron preparations (Table S8), so one number describes one object. The mouse value is the unweighted mean over the five naive iPain dorsal root ganglion datasets with at least 100 neurons (Table S4); the two datasets under that size, at 6 and 43 neurons, are printed in the same table rather than dropped, and neither enters the mean. The comparison is therefore across two pipelines as well as two averaging schemes, and is read as direction and rough scale rather than as a calibrated ratio.

Software and reproducibility

Analysis used Python 3.13 with h5py, NumPy and SciPy, and R 4.4.3 for the RDS objects; scripts are listed under Code availability. Every number quoted here is re-derived from the deposited supplementary tables by a single verification script that recomputes ratios, intervals, fold-changes and rounded values from the underlying counts.

Results

Three species, one laboratory: the dominant RAMP is species-dependent

The cleanest comparison in the system is GSE201654. In the CALCA gate the species fall on a magnitude gradient with exactly one qualitative step (Table 1, Figure 1).

Table 1. RAMP detection and allocation in the CALCA gate of GSE201654.

Measure	Human DRG	Macaque DRG	Mouse DRG
Samples (of listed)	18 / 18	16 / 16	10 / 10
Cells or nuclei in gate	20,852	57,032	27,430
Pooled median raw UMI	2,476	2,318	2,380
CALCRL	21.64	1.63	6.12
RAMP1	4.50	5.02	0.77
RAMP2	6.81	7.34	15.82
RAMP3	7.19	**39.41**	0.86
RAMP3 / RAMP2	**1.06**	**5.37**	**0.054**
RAMP1 / RAMP2	0.66	0.68	0.049
Paired RAMP3 vs RAMP2 (R3-only / R2-only)	1,113 / 1,032	**20,439 / 2,152**	170 / 4,275
Paired odds ratio (R2 over R3)	0.927 ($p = 0.084$)	**0.105 ($p < 10^{-300}$)**	**25.15 ($p < 10^{-300}$)**
Paired RAMP1 vs RAMP2 (R1-only / R2-only)	706 / 1,186	2,422 / 3,749	147 / 4,275
Paired odds ratio (R2 over R1)	1.680 ($p = 1.7 \times 10^{-28}$)	1.548 ($p = 2.1 \times 10^{-64}$)	**29.08 ($p < 10^{-300}$)**
Paired RAMP3 vs RAMP1 (R3-only / R1-only)	1,345 / 784	21,276 / 1,662	223 / 200
Paired odds ratio (R1 over R3)	0.583 ($p = 2.8 \times 10^{-34}$)	**0.078 ($p < 10^{-300}$)**	0.897 ($p = 0.285$)

CALCA+ cells; pooled median raw UMI 2,476 human / 2,318 macaque / 2,380 mouse. The CALCRL row is printed for completeness only. Absolute CALCRL in the human arm of this series is anomalous and is excluded from every abundance statement; the allocations below it are within-cell and do not depend on it.

Mouse neurons allocate the pool to RAMP2 over both competitors: 25.15 against RAMP3 and 29.08 against RAMP1, with all ten samples pointing that way and leave-one-out ranges of 23.7–29.3 and 26.3–31.2. Macaque neurons invert the first and keep the second: RAMP3 over RAMP2 at 0.105, a 239-fold gap in within-cell odds from mouse on the axis deciding between an AM2 and an AM1 receptor, while lying 19-fold away on RAMP1 versus RAMP2. The formal species × RAMP interaction on RAMP3/RAMP2 is a ratio of odds ratios of 0.0042 (95% CI 0.0036–0.0049, $z = -67.3$). Human neurons do neither: RAMP3 and RAMP2 show no detectable difference at 0.927 ($p = 0.084$), and the RAMP2 excess over RAMP1 is 1.68-fold where mouse gives 29-fold. These estimates count cells as independent. Resampling the 18, 16 and 10 sequencing samples leaves the interaction where it was, at 239 (bootstrap 95% CI 120–461), and widens the arms to 0.927 (0.694–1.536) in human, 0.105 (0.059–0.194) in macaque and 25.1 (18.6–34.6) in mouse (Table S24). At sample level RAMP3 versus RAMP2 and RAMP1 versus RAMP2 both survive, while human RAMP3 versus RAMP1 does not (0.583, 0.396–1.039), consistent with our not claiming it.

Macaque is not a large human: on RAMP3 versus RAMP1 the two differ 7.5-fold in odds ($z = +38.9$) and on RAMP3 versus RAMP2 by 8.8-fold ($z = +44.6$). What they share is the RAMP1-versus-RAMP2 axis, where their estimates are 1.680 and 1.548 (ratio of odds ratios 1.085, $z = +1.51$, $p = 0.131$), each 17- to 19-fold from mouse. We do not convert that into agreement, a non-significant difference not being evidence of equivalence. What the data support is a bound: on the log-odds scale the human–macaque difference is 0.082 (95% CI −0.024 to 0.188) against 2.851 for human–mouse and 2.933 for macaque–mouse, which puts the two primates at least 15-fold closer to each other than either is to mouse, all inside one laboratory, one pipeline and one annotation. The stricter neuron gate gives the same picture (1.615 and 1.651; difference −0.022, 95% CI −0.173 to 0.129, against 2.670 and 2.648).

One property of the human arm has to be stated. Its nuclei detect CALCRL in 21.64% of cells against 1.63% in macaque and 6.12% in mouse at matching depth, and its pseudobulk CALCRL is 184.83 CPM against 4.35–9.43 in macaque and 18.28–21.06 in mouse (Table S29), with a composition abnormal in the same direction (SNAP25 4.7–5.9-fold lower, PECAM1 2.3–3.1-fold higher, P2RY12 2.2–41.9-fold higher); freezing does not explain it, the macaque frozen-to-fresh ratio being only 2.17. That arm is excluded from every statement about CALCRL abundance. The allocation estimate is a ratio between two paralogues in the same nucleus, which an arm-wide inflation of a third gene does not enter, but the near-parity it produces is read with its composition in mind.

A reference atlas of 53,596 human neurons reproduces the human side

The three human datasets above are small and disagree on magnitude. The reference atlas described in Methods puts 53,596 human neurons behind the same contrast, and four of its nine datasets are independent of everything else analysed here (Table S27, Figure S9).

The RAMP3-versus-RAMP2 contrast points the same way in all nine. Odds ratios run from 0.011 to 0.431 and every p is below 10^{-4}. Pooled by DerSimonian–Laird the RAMP3-versus-RAMP2 estimate is 0.114 (95% CI 0.059–0.220) with I^2 of 98.8%, and restricted to the four independent network datasets 0.093 (0.056–0.154) with I^2 of 90.7%. Applying the same CALCA+ gate to the atlas gives 43,709 neurons with 13,346 RAMP3-only against 1,433 RAMP2-only cells. The magnitude is still not estimable and the heterogeneity is still large, but the direction is not in doubt.

At sample level, 30 of the 30 samples with usable identities give an odds ratio below 1 and 27 reach $p < 0.05$.

The atlas also supplies the preparation control the human side lacked: one of its four network datasets is whole-cell SMART-seq2 (1,598 somata, median 145,856 UMI) and the other three are nuclei. Whole cells give 0.061 and the largest nuclear dataset 0.072, both two orders of magnitude below parity with intervals that do not approach it. A nuclear-capture artefact would have to act in the opposite direction to produce that, and it does not.

What the atlas does not do is rescue RAMP1. Its RAMP1-versus-RAMP2 contrast sits near parity, at 0.893 across all neurons and 1.112 in the CALCA gate, but ranges from 0.133 to 1.795 across the nine datasets and is 1.012 ($p = 0.74$) in the largest of them, 38,605 neurons. A three-gene ordering cannot be built from these data in either species, and we do not build one.

The difference is a family-internal crossover, not a platform shift

The most serious objection is technical: that one pipeline captures RAMP3 more efficiently and inflates the primate-side values. An effect acting on the family as a whole, whether total capture, total RNA per cell or annotation completeness, must move all three RAMPs the same way, and the human-versus-mouse comparison violates that. Between dorsal root ganglion neurons, RAMP1 is 3.0-fold higher in human (3.45 vs 1.13) and RAMP3 12.3-fold higher (17.74 vs 1.44), but RAMP2 is 7.0-fold higher in mouse (3.57 vs 0.51). Pseudobulk counts give the same crossover on a continuous metric and put a scale on it (Methods; Tables S4 and S8): neuronal CALCRL is 8.13 CPM in human and 7.35 in mouse (1.11-fold), so the supply of receptor is comparable while

RAMP2 is 7.4-fold higher in mouse (5.59 against 0.753 CPM) and RAMP3 50-fold higher in human (52.39 against 1.05).

The same data rule out a constant per-dataset factor. If capture or annotation differed by one multiplicative constant, f would take a single value in every cell type. It does not: f spans 0.41–33.6 in the trigeminal ganglion (82-fold) and 0.20–150.8 in the dorsal root ganglion (740-fold), and it crosses 1, with fibroblasts agreeing between species (0.66 and 1.19) and immune cells inverting the direction seen in neurons (0.41 and 0.20) (Figure 3 and Table S11).

Two positive controls support comparability (Table S8). CALCA is detected at nearly identical rates in human dorsal root ganglion neurons (53.62%) and mouse trigeminal neurons (52.11%), a ratio of 1.03, and the non-neuronal ambient load in the two neuron gates is almost the same (PLP1 14.12% against 17.71%; PECAM1 5.76% against 6.83%), so the gates are equally pure.

One further comparison holds the pipeline fixed rather than correcting for it. In the trigeminal ganglion, 89% of the mouse neurons (23,779 of 26,667 nuclei) come from the mouse arm of GSE197289, the same series as our human trigeminal dataset, with the same cell-type vocabulary and barcode conventions. Detection is a property of the raw count matrix, not of any downstream pipeline, so this runs on two arms of one design and removes the between-study component of the objection entirely. It yields a second species × RAMP interaction with study, chemistry, ganglion and pipeline all held constant: mouse neurons from that series give 1.81 (336 RAMP3-only against 609 RAMP2-only) where human neurons from the same series give 0.145, a ratio of odds ratios of 12.5 (9.5–16.4, z = 18.2; Table S25). The mouse side sits close to parity, which is why the trigeminal ganglion does not carry the paper.

Depth, suspension and study identity do not produce the inversion

Depth was calibrated on a subtype in which the two species are matched. The PEP subtype has 6,606 median UMI in mouse and 6,792 in human (ratio 0.97) and needs essentially no correction: expected 1.82% against observed 1.67%, a factor of 1.09. Applied to the other subtypes the model is violated in every case, and for the NP subtype in the direction opposite to the artefact: mouse cells were sequenced 2.2-fold deeper than human cells yet detected Ramp3 124-fold less often (Table S6). The same contrast recomputed inside depth bins of the three-species series widens with depth rather than closing: in the deepest bin the human and macaque odds ratios are 1.140 and 0.072, a 15.9-fold separation (Figure 2b and Table S18). Dropping cell-level depth entirely, by pseudobulk aggregation and by the matched-subtype normalisation, leaves the difference in place (Figures S1 and S2), and the per-subtype detection rates behind the calibration are in Figure S3.

Suspension type fails in the same direction. In the mouse trigeminal ganglion, Ramp3 is scored in 2.16% of dissociated cells (n = 2,773) and 1.48% of nuclei (n = 23,894), a ratio of 0.68 (Figure S4). Nuclear capture would have to push nuclei higher, not lower; and at 1.5-fold the effect is an order of magnitude too small to explain a 10–30-fold gap. The matched comparison is already like-for-like, because both human datasets are nuclei-based.

Study identity was tested by repeating every mouse analysis inside each contributing study. In the dorsal root ganglion, six of eight studies reproduce RAMP2 > RAMP1 as a paired within-cell result, at p from 1.8×10^{-3} to 1.3×10^{-178}, across 10x cell-based, 10x nuclei-based, multiome and Smart-seq3 chemistries; one small study (n = 245) goes the other way (Table S4 and Figure S6). For the contrast this paper rests on, all seven testable studies agree that Ramp2 exceeds Ramp3, including the study that reverses RAMP1 versus RAMP2. Pooling the nuclei-based strata gives a within-cell odds ratio of 4.54 for RAMP2 over RAMP1 (95% CI 3.77–5.48; k = 5 strata; p = 2.3×10^{-56}; I^2 = 29.4%), which becomes 4.49 (4.00–5.04) with I^2 = 0.0% once its single zero-count stratum is removed. The human values are 0.59 (0.46–0.77) in the trigeminal ganglion and 0.13 (0.06–0.28) in the dorsal root ganglion, pooling to 0.293 (0.068–1.261) with I^2 of 92.9%; the interaction of the pooled mouse estimate of 4.54 against that pooled human value is a ratio of odds ratios of 15.5 (3.56–67.5, z = 3.65, p = 2.6×10^{-4}), and per ganglion 7.0-fold

in the trigeminal and 71-fold in the dorsal root ganglion, so the pooled figure is not doing work that either ganglion contradicts. A reader should nonetheless see that this is the one contrast whose pooled human interval reaches parity.

The atlas also pools disease models. Of its 117,284 dorsal root ganglion neurons, 24,702 are naive controls and the rest largely come from nerve crush, sciatic and spared nerve transection, paclitaxel, complete Freund's adjuvant, chronic constriction injury and sham surgery. Recomputing the primary contrast inside each condition leaves the direction untouched in every model with enough cells: RAMP2 exceeds RAMP3 at 3.40 in naive neurons, 2.51 in the non-naive aggregate, and between 1.31 and 5.00 in each individual model (Table S23). The naive subset is the stronger of the two, so the models dilute the contrast rather than create it. Satellite glia and the trigeminal ganglion behave the same way.

The limit of this must be stated as plainly. Pooling the mouse whole-cell strata does not reproduce the effect (odds ratio 1.80, 0.71–4.61, $p = 0.22$, $I^2 = 97.8\%$), and the heterogeneity is driven almost entirely by one study, which gives 0.04 against 3.2–11.9 in the other three cell-based dorsal root ganglion studies. We therefore do not claim that the RAMP2-over-RAMP3 contrast in mouse is independent of suspension type. We claim that in nuclei-based mouse data, the modality in which every human observation here was made, that contrast is consistent, homogeneous once the extreme stratum is dropped, and formally different from the human estimate.

The allocation replicates across macaque resources, species and chemistries

Three further macaque resources from a single laboratory had never been examined for RAMP allocation (Table 2, Figure 2a).

Table 2. RAMP3-versus-RAMP2 allocation in four macaque resources from two studies.

Resource	Species	Chemistry	Cells in gate	RAMP3-only / RAMP2-only	OR (95% CI), R2 over R3	Units favouring RAMP3
GSE201654	*M. fascicularis*	10x snRNA	57,032	20,439 / 2,152	**0.105** (0.101–0.110)	12 of 16 samples
GSE148238	*M. mulatta*	SmartSeq2	1,627	1,077 / 65	**0.060** (0.047–0.078)	2 of 2 plates
GSE165553	*M. mulatta*	SmartSeq2	1,130	386 / 209	**0.542** (0.458–0.641)	7 of 9 libraries
GSE165566	*M. mulatta*	WaferGen	2,518	1,752 / 71	**0.041** (0.032–0.051)	3 of 3 animals
All four	2 species	3 chemistries	62,307	23,654 / 2,497	NA	**24 of 30 units**

Odds ratios are within-cell, with 95% confidence intervals.

All four place RAMP3 above RAMP2 in the same cells, and 24 of the 30 constituent units (plates, animals, libraries and samples) do so individually. The three new resources are not independent replications of one another, being three datasets from one study, so the honest count of independent macaque studies is two rather than four; what they add is a second macaque species, a second laboratory and two further chemistries, which is what a species claim requires.

The comparison also demonstrates the design rather than asserting it. Across the four resources RAMP2 detection ranges from 7.34% to 42.92% (a 5.8-fold spread), and RAMP1 from 0.80% to 6.46% (an 8-fold spread), while RAMP3 stays within 1.9-fold. Pooled detection rates across these resources are therefore not comparable, while the within-cell odds ratio is unaffected, being computed from cells in which both genes were measured. Restricting the one resource whose gate was not purely expression-based to annotation-confirmed neurons (877 of 1,130 cells)

leaves every conclusion in place: 0.567 against 0.542 for RAMP3 versus RAMP2, and 10.35 against 9.77 for RAMP1 versus RAMP2.

The species × RAMP interaction is also not an effect of how the cells were prepared. Twenty-four stratum-by-gate combinations are populated in both species; one is not estimable, and in each of the other 23 the mouse odds ratio exceeds the macaque one, by 13- to 603-fold, with no combination approaching parity (Table S17).

Neighbouring compartments of one ganglion use different RAMPs

Using markers rather than atlas labels, the endothelium and the smooth muscle of the mouse dorsal root ganglion are distinct CALCRL compartments. Endothelium (n = 9,749) detects RAMP1 in 0.56% of cells and RAMP2 in 60.31%; the strict smooth-muscle gate (Myh11+, Cnn1+, neuronal markers absent) retains 294 cells and detects RAMP1 in 67.69% and RAMP2 in 9.52% (Figure 4). RAMP1 therefore differs 121-fold between two adjacent compartments of one ganglion, and the strict gate contains no neuronal-marker-positive cells while being 85% atlas-labelled smooth muscle, so this is not a doublet effect. Endothelial RAMP1 is likewise 0.56% in both the trigeminal (n = 3,726) and the dorsal root ganglion (n = 9,749), a property of sensory-ganglion endothelium rather than a trigeminal peculiarity, and the paired comparison gives RAMP2:RAMP1 ratios of 92.3 and 278.4 with 10 of 10 depth strata concordant (Figure S5).

That disposes of a possible artefact and explains the classical literature at once: CGRP dilates cranial vessels through smooth muscle, and classical preparations deliberately denuded the endothelium, coherent with that endothelium being an AM1 compartment. In the mouse trigeminal ganglion the equivalent test was not possible, the atlas smooth-muscle cluster (n = 443) being 89.6% neuronal-marker-positive with 8 cells surviving a strict gate; we report that as a gap.

The compartment the classical literature places the RAMP2/RAMP3 signal in, satellite glia, had never been measured on its own. It now has been, in two human resources and in the mouse atlas, and it points the same way (Figure 5 and Table S21).

In the mouse atlas the satellite-glial label detects RAMP2 in 47.48% of 22,613 dorsal root ganglion nuclei against 0.38% for RAMP1 and 0.19% for RAMP3, a within-cell odds ratio of 0.0019 for RAMP3 versus RAMP2 (10,713 RAMP2-only against 20 RAMP3-only cells); in the trigeminal ganglion the figure is 0.0044. All five contributing sources are RAMP2-first; splitting by suspension type leaves the direction untouched in both strata (17.83% in nuclei, n = 10,387; 72.66% in whole cells, n = 12,226) and splitting by disease state leaves it untouched as well (odds ratio 482 in naive cells against 559 in non-naive; Table S23). The label is glial on its own markers but leaky in both directions, as atlas labels are; that leakage cannot produce the RAMP2 rate, because the compartments it could come from are far lower (mouse neurons detect Ramp2 in 3.57%, pericytes in 9.85%).

In human tissue RAMP2 is minor in every glial gate of both datasets (0.16% to 3.84%) and undetected in the four tightest gates of the first. GSE310000 shows RAMP3-leaning glia (PLP1+ n = 2,708: RAMP3 10.16%, RAMP2 0.33%, odds ratio 39.0, 18.4–82.6), and the estimate survives exclusion of every SNAP25+ nucleus. GSE189501, a glia-focused preparation detecting SNAP25 in only 1.79% of nuclei and so not neuronally contaminated, leans RAMP1 instead (PLP1+ n = 4,478: RAMP1 5.69%, RAMP2 2.50%), and a third human resource agrees with it. The datasets therefore agree that RAMP2 is minor and disagree about the runner-up. The species gap on the RAMP2 column is at least 4.6-fold at the closest comparison and two orders of magnitude at the widest.

A rat arm on a whole-cell platform, and what the annotation audit found

One accession closed two gaps: the rodent literature that motivates this work was done in rat, which we had not analysed, and the cross-species comparisons this paper rests on were made in nuclei. GSE169301 supplies rat dorsal root ganglion on a whole-cell platform (papain/collagenase dissociation, FACS-selected live cells, 10x

Chromium) and six human single-nucleus libraries from the same study. The two arms share no platform and are therefore used as two directional replications, never as a rat-versus-human contrast (Table S22).

In the rat neuronal gate (3,461 cells) RAMP2 is detected in 13.49% of cells against 4.25% for RAMP3 and 3.81% for RAMP1; within the same cells RAMP2-only cells outnumber RAMP3-only cells 359 to 39 (odds ratio 9.21, 6.61–12.81) and RAMP1-only cells 382 to 47 (8.13, 6.00–11.00). In the glial gate (13,892 cells) the figures are 1,189 against 100 (11.89, 9.70–14.58) and 1,205 against 160 (7.53, 6.39–8.88). Rat sits on the rodent side of the inversion on both axes it can be tested on and in both compartments, so the rodent result is no longer a nuclear-preparation finding (Figure S7b). The human arm of the same series returns the direction of the other three human datasets (24 RAMP3-only against 13 RAMP2-only, odds ratio 0.54, 0.28–1.06, p = 0.099) and is not pooled with them, 598 cells at that depth contributing an order of magnitude fewer discordant pairs than the smallest of the three primary estimates.

The annotation audit was not a formality. The deposited file names of that series do not carry the species unambiguously, and read naively two of the six human libraries read as rat; a rat arm built that way would have pointed the human way and been reported as a species reversal. All six proved human on three independent checks (sample titles, 45,924 ENSG against 25,399 ENSRNOG identifiers, and MT-ATP6 against Mt-atp6 symbol style).

Ganglion shifts the magnitude

The two human ganglia do not agree on magnitude: trigeminal neurons give 0.145 and dorsal root neurons 0.019, so the dorsal root estimate is a ratio of odds ratios of 0.13 (0.06–0.31) against the trigeminal one. Mouse behaves the same way in the other direction, at 1.81 against 2.65 (1.46, 1.26–1.69), so ganglion moves the estimate several-fold in both species while leaving each on its own side of parity (Table S25). Every species contrast here is made within one ganglion, with one exception: mouse versus human on RAMP1 versus RAMP2 pools both ganglia on both sides. Per ganglion it points the same way and by a wider margin in both, at 4.165 against 0.592 in the trigeminal and 9.464 against 0.133 in the dorsal root ganglion (Table S13).

What does not replicate

Three results are reported as limits rather than findings. The trigeminal ganglion comparison is protocol-contingent: 89% of its mouse neurons come from one study, and the single whole-cell dataset (2,547 neurons) returns the human ordering, so the dorsal root ganglion is the study-robust result. The human RAMP1-versus-RAMP2 estimate is dataset-dependent across every human dataset (Table S27). And the deepest human dataset available does not settle the human question, because RAMP2 falls below the detection floor fixed before the file was opened (4.22%, against 40.05% for RAMP3; Table S20), so no paired estimate is claimed from it on either axis.

Discussion

The receptor that CALCRL builds in a sensory neuron is a species variable. Where macaque, human and mouse ganglia were prepared and sequenced together, mouse neurons give the pool to RAMP2 and macaque neurons give it to RAMP3, a 239-fold species × RAMP interaction that survives every preparation stratum. Human neurons point the way macaque neurons do in every dataset examined, all nine of the reference atlas included, but the estimates span more than an order of magnitude, so we report direction with a pooled interval rather than a single number. The pool itself is not what differs: neuronal CALCRL measures 8.13 CPM in human dorsal root ganglion neurons (GSE168243) against 7.35 across naive mouse samples (iPain), an 11% gap across two pipelines and two kinds of average, which cannot turn one partner into the majority when the two species order them oppositely: among cells in which exactly one of RAMP2 and RAMP3 was detected, RAMP2 accounts for 96% in mouse, 9.5% in macaque and 48% in human. And it is a crossover inside one gene family, RAMP1 and RAMP3 higher in human, RAMP2 higher in mouse.

The distinction is one abundance measurement cannot reach. A bulk sample averages neurons with glia and vascular tissue, and a per-gene detection rate in single cells says how many cells carry a transcript, not what it is partnered with: a neuron that doubles CALCRL and doubles every RAMP registers no change in either. The three RAMPs also behave as one coupled pool whose components move together [16], which is precisely the regime in which allocation is the informative quantity and abundance is not.

Every approved CGRP-pathway drug acts on the peptide or on CALCRL [4–11], and CGRP-targeted agents are now first-line preventive options [12]. Nothing here challenges their efficacy. It does constrain how that efficacy is explained, because the entity these drugs engage is defined by which RAMP is present, and that is the variable found to differ. If transcript-level allocation predicts the assembly a neuron presents, mouse and human sensory neurons do not present the same receptor. RAMP1, the partner that makes CALCRL a CGRP receptor, is lower in mouse than in human dorsal root ganglion neurons on both metrics, 3-fold on detection rate (1.13% against 3.45%) and 10-fold on pseudobulk CPM (0.54 against 5.42), and the dominant non-CGRP assembly is AM1 in mouse and AM2 in human. A rodent experiment that titrates a CGRP antagonist against sensory-neuron excitability therefore addresses a minority of the CALCRL in those cells. The amylin-1 assembly, calcitonin receptor with RAMP1, adds a second route [42]. None of this explains a clinical result by itself, but it is one candidate reason why CGRP-pathway antagonism is potent and dependable in rodent pain models while its clinical effect in migraine, though real, is partial.

If the CGRP partner is that much rarer in mouse, why is CGRP-pathway antagonism potent and dependable in rodent pain models? Three readings are open. Reserve is one: antagonist potency is not proportional to the fraction of neurons carrying the partner, because a minority of assemblies can support a full response where the effector is amplified downstream. A second is that we measure a frequency of cells, not a density of receptors on any one of them, so a sparse but densely expressing subpopulation would be invisible to a frequency statistic while dominating a pharmacology experiment. A third is that the CGRP response need not run through CALCRL with RAMP1 at all, the amylin-1 assembly of calcitonin receptor with RAMP1 being functional in the ganglion [42] and absent from both of our contrasts. That a mouse can be made to respond like a primate when human RAMP1 is expressed in it [18] argues the partner is limiting somewhere in the circuit without locating the step. Our numbers rule out the reading that rodent CGRP pharmacology must be weaker. What they support is a claim about which assembly a rodent result concerns.

The human side is no different, and the numbers invite the opposite conclusion there too: RAMP1 is a minority partner in human dorsal root ganglion neurons, 3.45% against 17.74% for RAMP3, so an account requiring the CGRP receptor to be the majority assembly fails here as well. Allocation says which assembly predominates in a population, not which one carries a response.

A species difference at this receptor was documented at the protein level long before anyone looked in transcripts. RAMP1 determines the species selectivity of non-peptide CGRP receptor antagonists, which is why compounds optimised against the human receptor proved weak at the rodent one [43, 44], and the mouse receptors differ further in antagonist affinity [45]. Our result is the transcript-level counterpart, and a receptor assembled around a different partner is unlikely to be pharmacologically interchangeable with the one the drugs were designed against.

The non-CGRP assemblies matter for the same reason. Adrenomedullin and adrenomedullin 2 are among the most frequently proposed non-CGRP targets in headache [20, 21], and in primate sensory neurons this pathway runs mainly through RAMP3, hence AM2, whereas in mouse neurons it runs through RAMP2, hence AM1. The two receptors differ in peptide preference and antagonist profile, so a rodent result about adrenomedullin in the ganglion does not transfer to the human ganglion by default. A harmonised cross-species atlas has already raised the possibility of species-level differences in these tissues [46]; what this work adds is allocation rather than abundance, resolved to the neuronal compartment.

The allocation model makes a prediction that no antibody is needed to test. If the transcript-level division of the pool predicts the assembly a neuron presents, then adrenomedullin should act on macaque and human sensory neurons predominantly through AM2 and on mouse and rat neurons through AM1, and a RAMP-directed antagonist should follow the same order. The two adrenomedullins differ in their preference for the two assemblies, so a peptide-order experiment on dissociated sensory neurons would separate those predictions with reagents that already exist. The complementary test is transcript-independent and harder: isoform-resolved protein measurement in the same cells, which the antibodies needed for it cannot currently deliver in characterised form [30], although the primate binding site has been localised with antagonist antibodies [27]. Until one of them is done, the human side of this comparison rests largely on nuclei, and a statement about which assembly a human neuron presents is an inference from allocation rather than an observation of it. We have kept that distinction visible wherever it bears on a conclusion, and a reader should hold us to it.

The design carries beyond this question. Comparing two paralogues inside one cell rather than two datasets makes depth and capture cancel by construction, and keeps the estimate defined where absolute detection differs several-fold between resources, as RAMP2 does across the macaque series. It does not measure three RAMPs competing for one pool, since co-detection of all three is rare here; it counts cells in which the two paralogues are scored oppositely. A platform artefact must act on the RAMP family as a whole, so a crossover within the family excludes that class of explanation at once, and a constant per-dataset factor is excluded by repeating the comparison across cell types, where f ranges over 740-fold and crosses 1. The annotation audit matters for a third reason: annotating a non-human library against the human transcriptome does not perturb a within-cell paralogue contrast, it can invert its sign.

The primate side rests on nuclear preparations; the rodent side no longer does. A rat dorsal root ganglion measured on a whole-cell platform reproduces the rodent direction in neurons and in glia [39], so a nuclear-capture artefact would have to be species-specific to survive, a narrower and less plausible claim. But the macaque arms remain nuclear in every dataset available and most human ones do too, and nuclei and whole cells are not interchangeable [40], so the human allocation is largely measured in the modality in which it is hardest to detect. The human arm of the three-species series is also compositionally abnormal and is excluded from every abundance claim. Closing the gap needs human whole-cell data at comparable depth. The reference atlas supplies one such library and returns the nuclear estimate; small as that arm is, it answers the objection in direction if not in precision.

Two explanations survive everything above. One is a gene-specific capture bias that happens to point in opposite directions in the two species; the other is a real difference in how the three RAMPs are transcribed. They are not equally weighted, since the first requires a coincidence that a crossover inside one gene family already makes unlikely, but our data do not formally separate them, and a protein-level test would.

The result is graded, and its shape carries information that the phrase species difference does not. Only the mouse crosses to the RAMP2-first side on the RAMP3-versus-RAMP2 axis; human and macaque differ on the other two axes while sitting on the same side of the RAMP1-versus-RAMP2 axis where both were measured together, an estimate that does not separate them, and the two primates examined here are at least 15-fold closer to each other than either is to mouse. Two histories would produce that pattern and these data cannot choose between them. If the ancestral state were RAMP3-leaning, the mouse is the derived case and the rodent an outlier; if it were RAMP2-leaning, the two primates are derived together and the mouse is the conservative one. Polarising the change needs a ganglion from a lineage that diverged before the primates, at the depth and quality these estimates require, and the public archives do not hold one. The difference is not academic: the first history weakens the mouse as a general model of this receptor, the second weakens the assumption that the primate arrangement is the general case. Nothing here tips the balance, and the claim we defend does not depend on which way it falls.

The same numbers show what a tissue-level assay would have reported. Pooling every cell class, human trigeminal ganglion gives 2.20 and mouse 21.0, and both would be called RAMP2-dominant, differing 9.6-fold; only when the

neuronal compartment is separated does human cross to the RAMP3 side. Whether the residual difference is biology or cell-type composition cannot be settled at that level.

The size of the human effect still cannot be estimated, though not for want of data. The three datasets analysed first give 0.019, 0.145 and 0.729 with I^2 of 99.1% (0.729 is that series' widest gate; its CALCA gate gives 0.927), and two are small enough that one sample drives the pooled estimate. The atlas adds nine datasets and 53,596 neurons, which narrow the direction to unanimity but leave the magnitude spread over an order of magnitude, at a pooled 0.114 (0.059–0.220) and I^2 of 98.8%. More human data has bought a firm direction, not a usable effect size.

Finally, the evidence is transcript-level throughout. No protein, membrane localisation or signalling was measured, and the antibodies needed to separate one CALCRL assembly from another are not available in characterised form, which is why the question had not been answered directly before [30]. Two human contrasts, RAMP2 at 0.51% detection in dorsal root ganglion neurons and 2.48% in trigeminal neurons, sit below the threshold at which the detection floor binds on full-length chemistries; their discordant counts are printed and their intervals narrow enough to be informative, but both should be read as directional. The exact tests also treat cells as independent, which the sample-level bootstrap bounds for the three-species series (Table S24) but not for atlas strata that do not expose per-donor counts. Genome-wide association data from more than 100,000 cases place a locus at the ligand genes CALCA and CALCB but no genome-wide significant signal at CALCRL, RAMP1, RAMP2, RAMP3 or ADM [47], so nothing here identifies a therapeutic target or explains a genetic signal; it identifies a difference in what the existing target is.

Conclusions

Receptor pharmacology has been organised around the assumption that a named receptor is the same molecule across mammals. For G-protein-coupled receptors that depend on an accessory protein, that assumption needs testing, and here it fails. Human, macaque and mouse sensory neurons all express CALCRL and, where it can be measured, in comparable amounts; they do not divide it the same way. Macaque neurons assign it mainly to RAMP3 and mouse neurons mainly to RAMP2, human neurons follow macaque in every human dataset now available, with a magnitude that is still not estimable, and the same split reappears in satellite glia and in an independent rat whole-cell preparation. The consequence is interpretive, not therapeutic. The CGRP assembly is a minority partner in both species, but the pool it competes in is not the same one: the dominant non-CGRP assembly is AM1 in rodent neurons and AM2 in primate neurons, so a rodent study of the sensory-neuron CGRP receptor, and a rodent study of adrenomedullin in the ganglion, each describe a receptor population composed differently from the one the corresponding human study addresses. Neither statement undermines the drugs in clinical use, which engage the circulating ligand or the CALCRL–RAMP1 assembly they were designed against; both bear on what a rodent result about this receptor means for a human one. The practical recommendation is not to set rodent work aside but to name the assembly a rodent result concerns, because with three RAMPs in one cell that is a measurable quantity rather than an assumption. The same audit can be run on any accessory-protein-dependent receptor whose species transfer is taken for granted.

List of abbreviations

ADM: adrenomedullin

AM1: adrenomedullin 1 receptor (CALCRL with RAMP2)

AM2: adrenomedullin 2 receptor (CALCRL with RAMP3)

CALCA: calcitonin gene-related peptide alpha gene

CALCRL: calcitonin receptor-like receptor

CGRP: calcitonin gene-related peptide

CI: confidence interval

cLTMR: C-fibre low-threshold mechanoreceptor

CPM: counts per million

DRG: dorsal root ganglion

FACS: fluorescence-activated cell sorting

GEO: Gene Expression Omnibus

I^2: proportion of variance between estimates attributable to heterogeneity

NF: neurofilament-heavy-chain-positive nociceptor subtype

PEP: peptidergic nociceptor subtype

RAMP: receptor activity-modifying protein

RNA: ribonucleic acid

TG: trigeminal ganglion

UMI: unique molecular identifier

Gene symbols follow the HUGO Gene Nomenclature Committee for human genes, with mouse and rat orthologues written in title case (Calcrl, Ramp1, Ramp2, Ramp3). Marker genes retain their approved symbols throughout, for example SNAP25, PRPH, PLP1, SOX10, S100B, PECAM1, MYH11 and CNN1.

Declarations

Ethics approval and consent to participate

Not applicable. This study is a re-analysis of publicly deposited, de-identified sequencing data; the accessions are listed under Availability of data and materials. No new animals were used, no human tissue was collected and no identifiable information was accessed.

Clinical trial number

Clinical trial number: not applicable.

Consent for publication

Not applicable. The manuscript contains no individual person's data in any form.

Availability of data and materials

All primary data are public and are listed under their accessions: GSE197289, GSE168243, GSE201654 with its SubSeries, GSE148238, GSE165553, GSE165566, GSE249746, GSE310000, GSE189501 and GSE169301. The human dorsal root ganglion reference atlas [41] is not deposited in GEO; we used the authors' public preprint release, and the derived quantities are in Table S27. Every derived quantity quoted in this manuscript is deposited as a tabulated supplementary file and is re-derived from the underlying counts by a single verification script rather than from text. No new sequencing data were generated.

Code availability

The analysis scripts, and the single verification script that re-derives every printed number from the deposited supplementary tables, are available from the corresponding author on reasonable request; because every input is a public accession listed above, any number in this paper can be regenerated without new data.

Competing interests

The authors declare that they have no competing interests.

Funding

This work received no specific grant from any funding agency in the public, commercial or not-for-profit sectors.

Authors' contributions

Tianjiao Li: conceptualisation, methodology, formal analysis, writing (original draft). Yuhan Liu: formal analysis, validation, visualisation. Lingxuan Li: formal analysis, data curation, visualisation. Chenwei Li: data curation, validation. Ye Li: data curation, investigation. Chaodong Wang: writing (review and editing), resources. Yun Wang: supervision, writing (review and editing). Yonghong Liu: supervision, writing (review and editing). Bo Sun: conceptualisation, supervision, project administration, writing (review and editing). All authors read and approved the final manuscript.

Acknowledgements

The authors thank the investigators who deposited the datasets re-analysed here, in particular the iPain consortium, the PRECISION Human Pain Network, and the authors of GSE197289, GSE168243, GSE201654, GSE148238, GSE165553, GSE165566, GSE249746, GSE310000, GSE189501 and GSE169301, for making their data publicly available.

Figure legends

Figure 1. Neuronal RAMP repertoire across eight dataset rows. The rows are listed in the order in which they appear in panel a: (1) human trigeminal ganglion, GSE197289, n = 3,873 neurons; (2) human dorsal root ganglion, GSE168243, n = 1,770; (3) macaque dorsal root ganglion, GSE201654 in its strictest neuron gate (SNAP25+ and PRPH+), n = 10,727; (4) mouse trigeminal ganglion, iPain nuclei, n = 23,894; (5) mouse dorsal root ganglion, iPain, n = 117,284; (6–8) the human, macaque and mouse arms of GSE201654 in the depth-matched CALCA gate, n = 20,852 / 57,032 / 27,430. (a) Detection rate of RAMP1, RAMP2 and RAMP3 inside neurons. (b) Within-cell allocation of the CALCRL pool, as the proportion of cells positive for each RAMP among cells positive for any of the three; the number printed inside a column is that column's largest segment, in percent. (c) The ratio of detection rates for two pairs of paralogues, with four rows annotated; RAMP3/RAMP2 separates macaque from mouse by two orders of magnitude and also separates the two primates from one another, RAMP1/RAMP2 separates both primates from mouse, and only on that second axis do the two primates sit close together. Panels a to c are all depth-sensitive summaries and are shown for orientation; the within-cell odds ratio, which does not depend on depth, is the statistic this paper rests on and is reported in Table 1 and Figure 2.

Figure 2. The macaque replication and the depth test. (a) Four-resource forest plot of the RAMP3-versus-RAMP2 within-cell odds ratio with 95% confidence intervals, the discordant counts and the RAMP2 detection rate of each resource printed to the right of every row: the two quantities that move together under a capture explanation and here move apart. The RAMP1-versus-RAMP2 contrast is drawn one row below its resource and omitted for the two resources in which one of the two genes falls below the 5% detection floor that applies to full-length chemistries, where it is therefore not claimed. (b) RAMP3-versus-RAMP2 odds ratio by sequencing-depth bin for the three species of GSE201654, log axis, with the 15.9-fold deepest-bin separation annotated.

Figure 3. The species difference is cell-type-specific, not a single platform factor. For each cell type present in both species, f = (RAMP1/RAMP2)human ÷ (RAMP1/RAMP2)mouse, on a log axis on which a constant capture or annotation bias would place every cell type at one value; the dashed line is parity, f = 1. The observed values span 0.20 to 150.8 (740-fold) and cross that line, with fibroblasts agreeing between species and immune cells inverting the direction seen in neurons. Dot area encodes the smaller of the two cell counts entering each f, so an estimate resting on a thin gate shows up as a small dot: the endothelial value relies on 1,362 human cells against the 10,293 behind the satellite-glial one.

Figure 4. Adjacent vascular compartments use opposite RAMPs. (a) Mouse dorsal root ganglion, four gates in order of how much mural signal they admit: endothelium (PECAM1+) is RAMP2-dominant at 0.56% against 60.31%, pericytes (n = 3,776) are intermediate at 5.72% against 9.85%, the Myh11+/Tagln+ mural gate (n = 2,146) has already reversed the order at 36.53% against 16.26%, and genuine smooth muscle identified by markers alone (MYH11+ and CNN1+ and negative for neuronal markers, n = 294) is RAMP1-dominant at 67.69% against 9.52%; RAMP1 therefore differs 121-fold between the first and the last of these gates. (b) Mouse trigeminal ganglion: mural cells are also RAMP2-type, and there is no genuine smooth-muscle population large enough to test (n = 8), which is reported as a gap rather than a result.

Figure 5. The satellite-glial compartment. (a) RAMP1, RAMP2 and RAMP3 detection rates in satellite glia of mouse dorsal root ganglion and mouse trigeminal ganglion (atlas label, with the nuclei and whole-cell strata shown separately) against the marker-gated glial populations of the two human dorsal root ganglion datasets; RAMP2 is the only RAMP that separates the species in this compartment. (b) Within-cell RAMP3-versus-RAMP2 odds ratio for the same rows on a log axis, with 95% confidence intervals and discordant counts. The rows sit at the same vertical positions as in panel a and carry no labels of their own; the human trigeminal ganglion atlas row has no point because no per-cell file is deposited for it.

Supplementary figure legends

Figure S1. Depth-free and pseudobulk re-analysis of the primary datasets. The allocation difference survives when cell-level depth is removed entirely.

Figure S2. The matched-subtype depth-normalisation model. The PEP subtype is the calibration anchor, whose depths are matched and whose required correction is therefore essentially null.

Figure S3. Per-subtype detection of the three RAMPs across species. Heatmap, with the neuronal subtypes mapped one-to-one between taxonomies.

Figure S4. Suspension control in the mouse trigeminal ganglion. The RAMP3 share of dissociated cells against nuclei is the comparison that would have to run the other way for nuclear capture to explain the species difference.

Figure S5. The endothelial compartment. RAMP2 dominates in both species and the AM1-type assembly is the majority one, contrasting with the adjacent smooth muscle and neuronal compartments.

Figure S6. Per-study robustness of the mouse allocation. The within-cell contrast is recomputed inside each contributing study and split by suspension type.

Figure S7. Depth-matched detection and the rat arm. The first panels match cells on total UMI before comparing detection rates across species; the final panel gives the rat and whole-cell replication as a forest plot.

Figure S8. The neuronal and satellite-glial gates on the deposited atlas embedding. Mouse trigeminal (a) and dorsal root ganglion (b). Cells assigned to each gate by this study's markers are coloured and all remaining atlas labels are grey. The embedding is shown to document the gates; no quantity in this paper is measured from it.

Figure S9. The nine datasets of the human reference atlas. Each is drawn with its within-cell RAMP3-versus-RAMP2 odds ratio and 95% confidence interval on a log scale, ordered by effect size. The two filled diamonds are DerSimonian–Laird random-effects pools, one for the four independent network datasets ($k = 4$, $I^2 = 90.7\%$) and one for all nine ($k = 9$, $I^2 = 98.8\%$). Every row lies below parity, so the width of the pooled intervals describes a spread in magnitude rather than any disagreement about direction. Numbers at the right are the neurons entering each row.

Supplementary table legends

Table S0. Dataset screening record. Every GEO record returned by the title-field search of 18 October 2026, with the reason each record was included or excluded.

Table S1. Dataset summary. Accessions, platforms, sample counts and per-sample annotations. Median UMI is taken from the raw counts, not from the log-normalised matrix.

Table S2. Paired exact McNemar test for RAMP1 versus RAMP2 in the same cells, reported separately for every cell class.

Table S2b. Companion contrast to Table S2: paired exact McNemar test for RAMP3 versus RAMP2.

Table S3. Depth-decile stratified comparison of RAMP1 versus RAMP2. Deciles are computed from the raw counts, so a contrast that holds in every stratum cannot be a depth effect.

Table S4. Per-study mouse detection rates with Cochran's Q and I^2 for between-study heterogeneity, plus per-source pseudobulk CPM.

Table S5. Per-subtype sequencing depth and RAMP detection. Mouse rows are split by suspension because the iPain atlas contains both nuclei and whole cells.

Table S6. Matched-subtype depth-normalisation model, with the deficit factor computed on underlying transcript rates rather than on saturated detection fractions.

Table S7. Marker-gated vascular compartments in mouse trigeminal and dorsal root ganglion, with the doublet burden of each gate.

Table S8. GSE168243 per-preparation pseudobulk CPM, with GAPDH included as a positive control.

Table S9. Matrix audit. Detection counts from the two stored matrix forms over a fixed gene panel, in both iPain objects.

Table S10. Per-source paired tests within each contributing study and suspension stratum, with the true median raw UMI of each stratum.

Table S11. Cross-cell-type concordance: the ratio $f = (\text{RAMP1}/\text{RAMP2})_{\text{human}} \div (\text{RAMP1}/\text{RAMP2})_{\text{mouse}}$ computed for each matched cell type.

Table S12. Source composition of the iPain trigeminal and dorsal root ganglion atlases, with GEO accessions and suspension type.

Table S13. Pooled effect size and between-study heterogeneity for the within-cell RAMP contrast, pooled by DerSimonian–Laird random effects.

Table S14. Paired exact McNemar tests for the three RAMP paralogue contrasts in GSE201654, computed on the per-sample matrices of one laboratory and one pipeline.

Table S15. Across-species contrast of the within-cell RAMP paralogue ratios, for all contrasts and all gates, with the species × RAMP interaction.

Table S16. Per-sample leave-one-out robustness of every pooled GSE201654 estimate, with the ambient-RNA proxy of each sample.

Table S17. Preparation and purity stratification of the three-species GSE201654 contrasts, including the overlapping-purity window.

Table S18. Depth-response of the RAMP family within a single chemistry.

Table S19. The macaque RAMP3-dominant allocation across the four resources, resource by resource.

Table S20. GSE249746, human dorsal root ganglion single-soma deep RNA sequencing: detection-floor probe.

Table S21. The satellite-glial compartment, with the human and mouse gates reported side by side.

Table S22. The rat and whole-cell arm, together with the third human glial dataset.

Table S23. State invariance. The primary within-cell contrast recomputed inside every condition present in the atlas.

Table S24. Sample-level bootstrap of the GSE201654 comparison, resampling sequencing samples rather than cells.

Table S25. Ganglion, resolution and study controls for the RAMP3-versus-RAMP2 contrast.

Table S26. The guinea-pig arm of GSE201654: gene-model audit and exclusion.

Table S27. Release structure of the human dorsal root ganglion reference atlas, with the within-cell allocation estimate of each of its datasets.

Table S28. Joint detection of RAMP1, RAMP2 and RAMP3 in the same cell.

Table S29. Cell-weighted CPM for the three arms of GSE201654, with the absolute counts of the human arm disclosed as a within-series check only.

References

1. Goadsby PJ, Holland PR, Martins-Oliveira M, Hoffmann J, Schankin C, Akerman S. Pathophysiology of migraine: a disorder of sensory processing. *Physiol Rev* 2017;97(2):553–622.
2. Ashina M, Hansen JM, Do TP, Melo-Carrillo A, Burstein R, Moskowitz MA. Migraine and the trigeminovascular system: 40 years and counting. *Lancet Neurol* 2019;18(8):795–804.
3. Iyengar S, Johnson KW, Ossipov MH, Aurora SK. CGRP and the trigeminal system in migraine. *Headache* 2019;59(5):659–681.
4. Dodick DW, Silberstein SD, Bigal ME, Yeung PP, Goadsby PJ, Blankenbiller T, et al. Effect of fremanezumab compared with placebo for prevention of episodic migraine: a randomized clinical trial. *JAMA* 2018;319(19):1999–2008.
5. Stauffer VL, Dodick DW, Zhang Q, Carter JN, Ailani J, Conley RR. Evaluation of galcanezumab for the prevention of episodic migraine: the EVOLVE-1 randomized clinical trial. *JAMA Neurol* 2018;75(9):1080–1088.
6. Lipton RB, Goadsby PJ, Smith J, Schaeffler BA, Biondi DM, Hirman J, et al. Efficacy and safety of eptinezumab in patients with chronic migraine: PROMISE-2. *Neurology* 2020;94(13):e1365–e1377.
7. Goadsby PJ, Reuter U, Hallström Y, Broessner G, Bonner JH, Zhang F, et al. A controlled trial of erenumab for episodic migraine. *N Engl J Med* 2017;377(22):2123–2132.
8. Tepper S, Ashina M, Reuter U, Brandes JL, Doležil D, Silberstein S, et al. Safety and efficacy of erenumab for preventive treatment of chronic migraine: a randomised, double-blind, placebo-controlled phase 2 trial. *Lancet Neurol* 2017;16(6):425–434.

9. Dodick DW, Lipton RB, Ailani J, Lu K, Finnegan M, Trugman JM, et al. Ubrogepant for the treatment of migraine. *N Engl J Med* 2019;381(23):2230–2241.
10. Croop R, Goadsby PJ, Stock DA, Conway CM, Forshaw M, Stock EG, et al. Efficacy, safety, and tolerability of rimegepant orally disintegrating tablet for the acute treatment of migraine: a randomised, phase 3, double-blind, placebo-controlled trial. *Lancet* 2019;394(10200):737–745.
11. Pozo-Rosich P, Ailani J, Ashina M, Goadsby PJ, Lipton RB, Reuter U, et al. Atogepant for the preventive treatment of chronic migraine (PROGRESS): a randomised, double-blind, placebo-controlled, phase 3 trial. *Lancet* 2023;402(10404):775–785.
12. Charles AC, Digre KB, Goadsby PJ, Robbins MS, Hershey A; American Headache Society. Calcitonin gene-related peptide-targeting therapies are a first-line option for the prevention of migraine: an American Headache Society position statement update. *Headache* 2024;64(4):333–341.
13. McLatchie LM, Fraser NJ, Main MJ, et al. RAMPs regulate the transport and ligand specificity of the calcitonin-receptor-like receptor. *Nature* 1998;393:333–339.
14. Hay DL, Garelja ML, Poyner DR, Walker CS. Update on the pharmacology of calcitonin/CGRP family of peptides: IUPHAR Review 25. *Br J Pharmacol* 2018;175:3–17.
15. Hay DL, Walker CS, Gingell JJ, Ladds G, Reynolds CA, Poyner DR. Receptor activity-modifying proteins; multifunctional G protein-coupled receptor accessory proteins. *Biochem Soc Trans* 2016;44(2):568–573.
16. Holm A, Edvinsson JCA, Krause DN, Edvinsson L. RAMP1-dependent hormonal regulation of CGRP and its receptor in the trigeminal ganglion. *J Headache Pain* 2025;26(1):142.
17. Muff R, Leuthäuser K, Bühlmann N, Foord SM, Fischer JA, Born W. Receptor activity modifying proteins regulate the activity of a calcitonin gene-related peptide receptor in rabbit aortic endothelial cells. *FEBS Lett* 1998;441(3):366–368.
18. Bohn KJ, Li B, Huang X, Mason BN, et al. CGRP receptor activity in mice with global expression of human receptor activity modifying protein 1. *Br J Pharmacol* 2017;174(12):1826–1840.
19. Sisakht M, Khoshdel Z, Mahmoodazdeh A, Shafiee SM, et al. Adrenomedullin increases cAMP accumulation and BDNF expression in rat DRG and spinal motor neurons. *Iran J Basic Med Sci* 2021;24(7):978–985.
20. Al-Hassany L, Boucherie DM, Creeney H, van Drie RWA, Farham F, Favaretto S, et al. Future targets for migraine treatment beyond CGRP. *J Headache Pain* 2023;24(1):76.
21. Rees TA, Hendrikse ER, Hay DL, Walker CS. Beyond CGRP: the calcitonin peptide family as targets for migraine and pain. *Br J Pharmacol* 2022;179(3):381–399.
22. Cargnin S, Pautasso C, Viana M, Sances G, Mittino D, Cantello R, et al. Association of RAMP1 rs7590387 with the risk of migraine transformation into medication overuse headache. *Headache* 2015;55(5):658–668.
23. Walker CS, Hay DL. CGRP in the trigeminovascular system: a role for CGRP, adrenomedullin and amylin receptors? *Br J Pharmacol* 2013;170(7):1293–1307.
24. Edvinsson L, Grell AS, Warfvinge K. Expression of the CGRP family of neuropeptides and their receptors in the trigeminal ganglion. *J Mol Neurosci* 2020;70(6):930–944.
25. Lennerz JK, Rühle V, Ceppa EP, Neuhuber WL, Bunnett NW, Grady EF, Messlinger K. Calcitonin receptor-like receptor (CLR), receptor activity-modifying protein 1 (RAMP1), and calcitonin gene-related peptide (CGRP) immunoreactivity in the rat trigeminovascular system: differences between peripheral and central CGRP receptor distribution. *J Comp Neurol* 2008;507(3):1277–1299.
26. Cottrell GS, Roosterman D, Marvizon JC, Song B, et al. Localization of calcitonin receptor-like receptor and receptor activity modifying protein 1 in enteric neurons, dorsal root ganglia, and the spinal cord of the rat. *J Comp Neurol* 2005;490(3):239–255.
27. Miller S, Liu H, Warfvinge K, Shi L, et al. Immunohistochemical localization of the calcitonin gene-related peptide binding site in the primate trigeminovascular system using functional antagonist antibodies. *Neuroscience* 2016;328:165–183.
28. Rees TA, Russo AF, O'Carroll SJ, Hay DL, et al. CGRP and the calcitonin receptor are co-expressed in mouse, rat and human trigeminal ganglia neurons. *Front Physiol* 2022;13:860037.

29. Maddahi A, et al. Sex differences in expression of CGRP family of receptors and ligands in the rat trigeminal ganglion. *J Headache Pain* 2024;25:193.
30. Hendrikse ER, Bower RL, Hay DL, Walker CS. Molecular studies of CGRP and the CGRP family of peptides in the central nervous system. *Cephalalgia* 2019;39(3):403–419.
31. Yang L, Xu M, Bhuiyan SA, et al. Human and mouse trigeminal ganglia cell atlas implicates multiple cell types in migraine. *Neuron* 2022;110(11):1806–1821.e8.
32. Nguyen MQ, von Buchholtz LJ, Reker AN, Ryba NJ, Davidson S. Single-nucleus transcriptomic analysis of human dorsal root ganglion neurons. *eLife* 2021;10:e71752.
33. Techameena P, Feng X, Zhang K, Hadjab S, et al. The single-cell transcriptomic atlas iPain identifies senescence of nociceptors as a therapeutical target for chronic pain treatment. *Nat Commun* 2024;15:8585.
34. Jung M, Dourado M, Maksymetz J, Jacobson A, Laufer BI, Baca M, Foreman O, Hackos DH, Riol-Blanco J, Kaminker JS. Cross-species transcriptomic atlas of dorsal root ganglia reveals species-specific programs for sensory function. *Nat Commun* 2023;14:366.
35. Kupari J, Usoskin D, Parisien M, Lou D, Hu Y, Fatt M, et al. Single cell transcriptomics of primate sensory neurons identifies cell types associated with chronic pain. *Nat Commun* 2021;12:1510.
36. Yu H, Nagi SS, Usoskin D, Hu Y, Kupari J, Bouchatta O, et al. Leveraging deep single-soma RNA sequencing to explore the neural basis of human somatosensation. *Nat Neurosci* 2024;27:2326–2340.
37. Xu J, Li Y, Novak C, Lee M, Yan Z, Bang S, et al. Mitochondrial transfer from glia to neurons protects against peripheral neuropathy. *Nature* 2026;650(8103):951–960.
38. Zhang D, Wei Y, Chen Y, Chen H, Li J, Yang Y, Zhou C. Single-nucleus transcriptomic atlas of glial cells in human dorsal root ganglia. *Anesthesiol Perioper Sci* 2023;1:17. doi:10.1007/s44254-023-00015-5.
39. Avraham O, Chamessian A, Feng R, Yang L, Halevi AE, Moore AM, Gereau RW 4th, Cavalli V. Profiling the molecular signature of satellite glial cells at the single cell level reveals high similarities between rodents and humans. *Pain* 2022;163(12):2348–2364. doi:10.1097/j.pain.0000000000002628. PMID 35503034.
40. Ding J, Adiconis X, Simmons SK, Kowalczyk MS, Hession CC, Marjanovic ND, et al. Systematic comparison of single-cell and single-nucleus RNA-sequencing methods. *Nat Biotechnol* 2020;38(6):737–746.
41. Bhuiyan SA, Nagi SS, Sankaranarayanan I, Semizoglou E, Usoskin D, Yang L, et al. A reference atlas of the human dorsal root ganglion. *bioRxiv* 2025. doi:10.1101/2025.11.05.686654 [Preprint].
42. Walker CS, Eftekhari S, Bower RL, Wilderman A, Insel PA, Edvinsson L, Waldvogel HJ, Jamaluddin MA, Russo AF, Hay DL. A second trigeminal CGRP receptor: function and expression of the AMY1 receptor. *Ann Clin Transl Neurol* 2015;2(6):595–608.
43. Mallee JJ, Salvatore CA, LeBourdelles B, et al. Receptor activity-modifying protein 1 determines the species selectivity of non-peptide CGRP receptor antagonists. *J Biol Chem* 2002;277:14294–14298.
44. Hershey JC, Corcoran HA, Baskin EP, Salvatore CA, et al. Investigation of the species selectivity of a nonpeptide CGRP receptor antagonist using a novel pharmacodynamic assay. *Regul Pept* 2005;127(1–3):71–77.
45. Garelja ML, Bower RL, Brimble MA, Chand S, Harris PWR, Jamaluddin MA, et al. Pharmacological characterisation of mouse calcitonin and calcitonin receptor-like receptors reveals differences compared with human receptors. *Br J Pharmacol* 2022;179(3):416–434.
46. Bhuiyan SA, Xu M, Yang L, et al. Harmonized cross-species cell atlases of trigeminal and dorsal root ganglia. *Sci Adv* 2024;10(25):eadj9173.
47. Hautakangas H, Winsvold BS, Ruotsalainen SE, et al. Genome-wide analysis of 102,084 migraine cases identifies 123 risk loci and subtype-specific risk alleles. *Nat Genet* 2022;54:152–160.

Figures

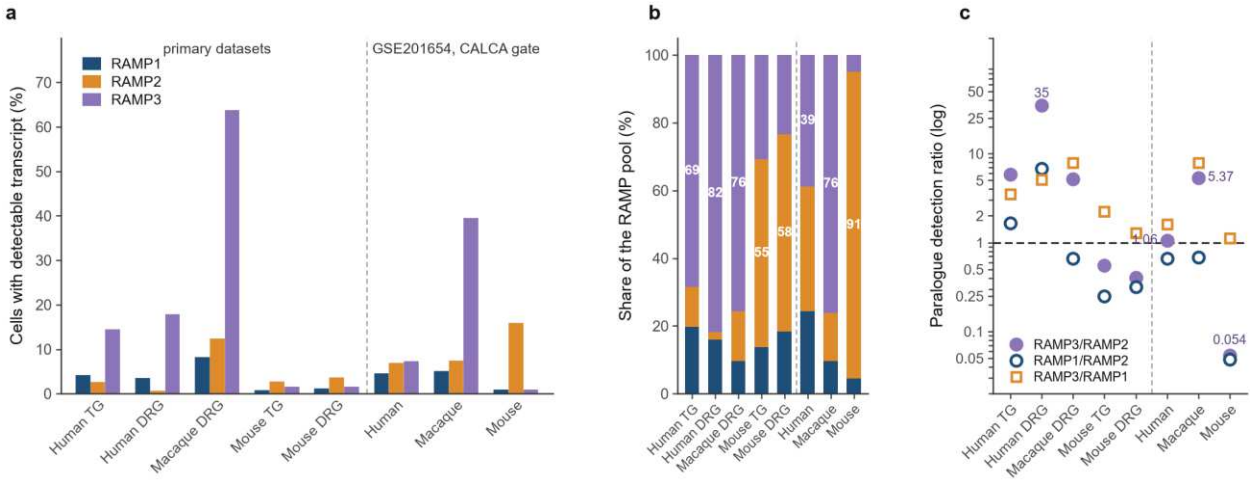
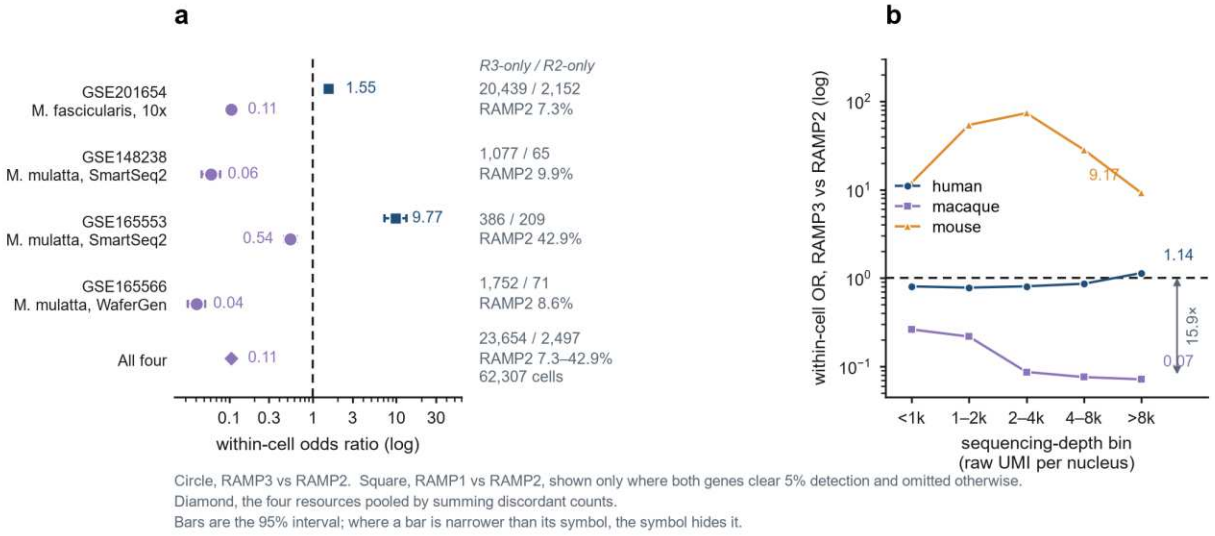


Figure 1.



Circle, RAMP3 vs RAMP2. Square, RAMP1 vs RAMP2, shown only where both genes clear 5% detection and omitted otherwise.
Diamond, the four resources pooled by summing discordant counts.
Bars are the 95% interval; where a bar is narrower than its symbol, the symbol hides it.

Figure 2.

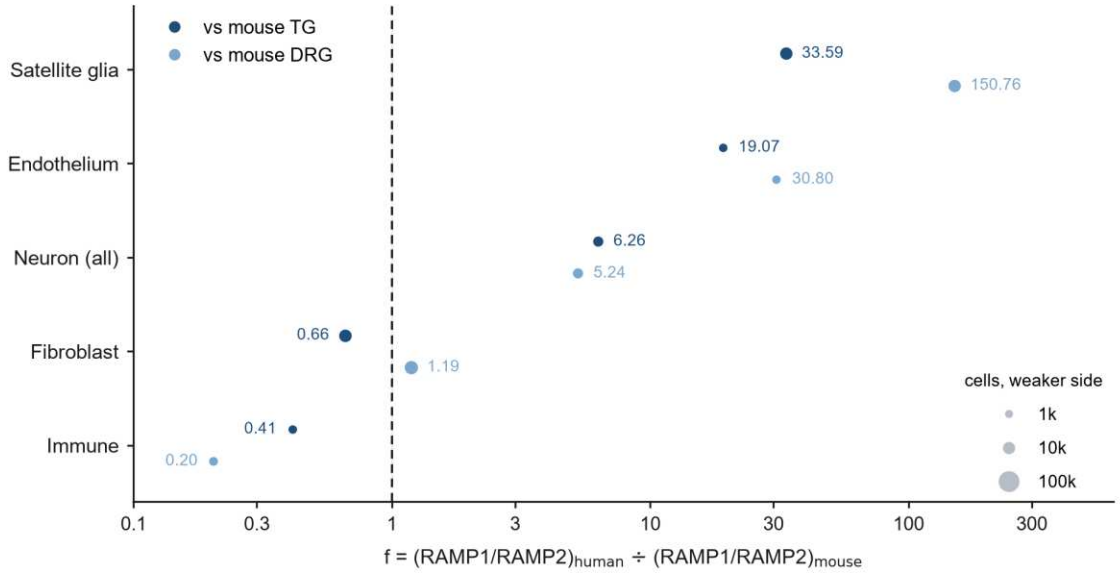


Figure 3.

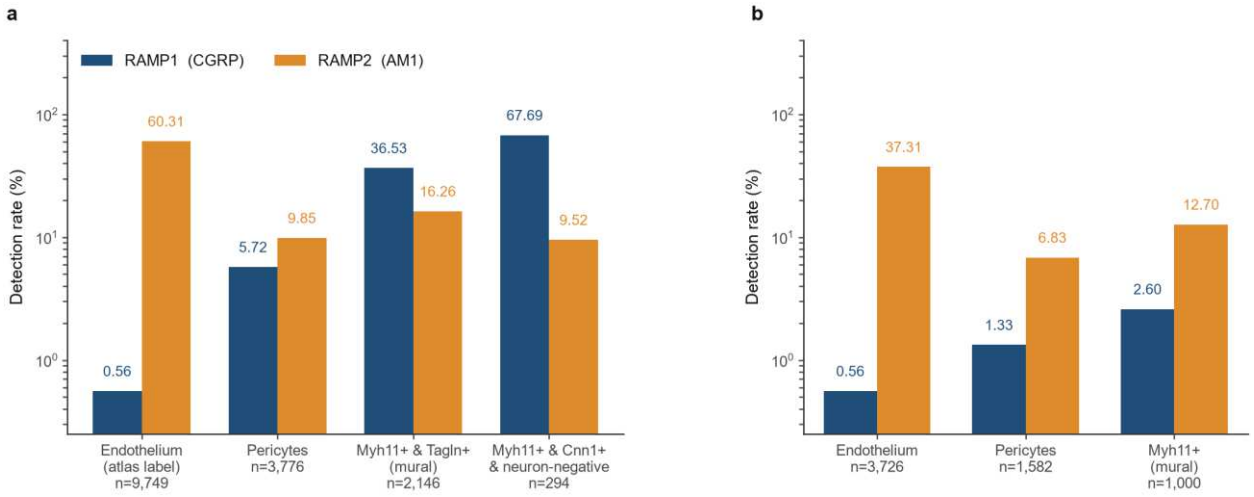


Figure 4.

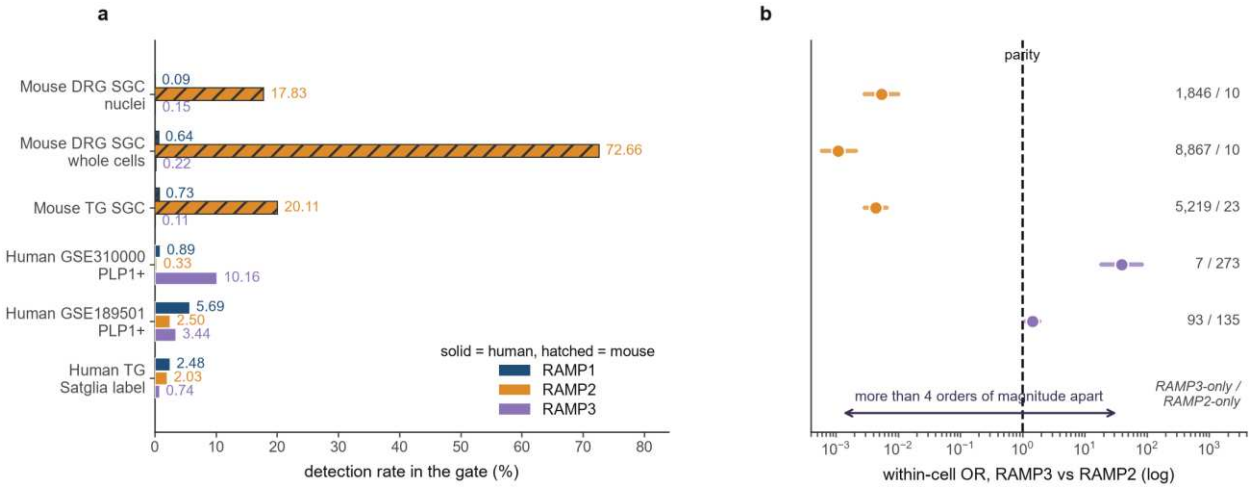

a
Mouse DRG SGC nuclei
0.09
17.83
0.15
Mouse DRG SGC whole cells
0.64
72.66
0.22
Mouse TG SGC
0.73
20.11
0.11
Human GSE310000 PLP1+
0.89
0.33
10.16
Human GSE189501 PLP1+
5.69
2.50
3.44
Human TG Satglia label
2.48
2.03
0.74
solid = human, hatched = mouse
RAMP1
RAMP2
RAMP3
0 10 20 30 40 50 60 70 80
detection rate in the gate (%)
b
parity
1,846 / 10
8,867 / 10
5,219 / 23
7 / 273
93 / 135
more than 4 orders of magnitude apart
RAMP3-only / RAMP2-only
10^{-3} 10^{-2} 10^{-1} 10^{0} 10^{1} 10^{2} 10^{3}
within-cell OR, RAMP3 vs RAMP2 (log)

Figure 5.

Supplementary Files

This is a list of supplementary files associated with this preprint. Click to download.

- 04SupplementaryTablesS0S29.xlsx
- 03SupplementaryFigures.docx